Advances in Science and Technology Research Journal

Advances in Science and Technology Research Journal, 2026, 20(5), 143–158
https://doi.org/10.12913/22998624/215591
ISSN 2299-8624, License CC-BY 4.0

Received: 2025.10.27
Accepted: 2026.03.15
Published: 2026.04.01

Research on the influence of the properties of mining sealing materials

Xianggui Tian[1,2], Deqian He[2,3*], Fuzhi Zhu[1,2], Shuqi Xu[2,3]

[1] Guizhou Energy Industry Research Institute Co., Ltd.,No. 48 Dazhi Road, Huaxi District, Guiyang City, Guizhou Province, 550025, China
[2] The Laboratory of Guizhou Province of Intelligent Development and Efficient Utilization of Energy, Guiyang 550025, China
[3] Mining College, Guizhou University, Guiyang 550025, China
* Corresponding author's e-mail: 15718621845@163.com

ABSTRACT

In order to improve the efficiency of coalbed methane extraction and reduce the risk of coal and gas outburst accidents, the modification of conventional sealing materials was carried out in this study, and the fly ash-cement-based mine sealing materials with nano-material composite were successfully developed. Focusing on the problem of leakage in coalbed methane extraction boreholes, the optimisation direction of sealing material performance is clearly proposed. The modification of cement-based sealing materials by nanomaterials was systematically studied, and the mechanism of action was revealed. The experimental data show that when the content of nano-SiO_2 and nano-metakaolin is 2% and 5%, respectively, the comprehensive properties of the materials reach the optimum, and the two nanomaterials achieve a synergistic enhancement effect through defect complementation. With the help of XRD, TG, MIP and SEM, it is clarified that nanomaterials can improve their properties by promoting hydration reactions rather than generating new products. The engineering application verification shows that the nanocomposite sealing material can significantly improve the gas extraction efficiency compared with the traditional materials.

Keywords: nano-silica, nanometakaolin, mining sealing materials, macro performance, microstructure.

INTRODUCTION

In 2024, China's raw coal output will reach 4.78 billion tons, up 1.2% year-on-year, accounting for 53.2% of the country's total energy consumption, down 1.6 percentage points from the previous year [1–3]. As a green and low-carbon form of energy, coalbed methane is a valuable unconventional natural gas that mainly occurs in coal seams and adjacent rock formations, and is gradually becoming a key part of the global energy structure transformation [4–7]. However, with the advancement of coal seam mining to deeper depths, the pressure and content of coal seam gas have increased significantly due to complex geological conditions, which poses a threat to the safety and stability of coalbed methane mining operations [2,8]. Effective exploitation of coalbed methane can not only alleviate the contradiction between energy supply and demand, but also significantly reduce the risk of potential gas escape in coal seams while improving the comprehensive utilisation efficiency of energy. The selection and application of sealing materials are crucial to reduce the microscopic cracks in the sealing process and improve the efficiency of coalbed methane exploitation [9–12]. There are two main ways to improve the efficiency of coalbed methane exploitation: (1) hydraulic fracturing and coal seam water injection are used to solve the problems of low permeability, small pore structure and excessive adsorption capacity of coalbed methane; (2) gas escape channels can be formed during drilling operations, and the number of

channels can be reduced through the application of sealing materials to improve the extraction efficiency of coalbed methane [13–15].

The sealing materials are used as a method to improve the efficiency of coalbed methane exploitation, and the widely used sealing materials mainly include polyurethane materials, high-water materials and cement-based materials [16, 17]. The polyurethane material has the advantages of light weight, easy expansion and simple construction operation, but the air permeability is poor, it is difficult to penetrate into the cracks around the wellbore, and it is difficult to form a stable supporting effect on the wellbore due to its low strength and easy deformation after compression, and the expansion proportion of the material is large in the foaming process, which may cause insufficient depth of the sealing layer and increase the risk of air leakage. With the increase of the water-cement ratio, the mechanical strength and durability of high-water materials will be reduced correspondingly, but the fluidity and permeability of the slurry will be improved, but the sealing efficiency of such materials may gradually decay after long-term erosion by the natural environment, affecting their long-term stability [18–20]. Cementitious materials are widely used in the field of downhole drilling and sealing due to their cost advantages and flexibility to adjust properties through admixtures [21–23]. Relevant studies have shown that the comprehensive performance of cement-based sealing materials can be significantly improved by adopting new admixtures, nanomaterial modification, fibre reinforcement technology, and formulation optimisation [24–26].

In order to further improve the performance of mineral-based sealing materials, experts and scholars have conducted extensive research and found that the comprehensive performance of mineral-based sealing materials can be significantly enhanced by introducing new additives, nanomaterials, fibre reinforcement technology and optimising formula design [27–28]. Fly ash is thought to increase the long-term properties of cementitious materials, but has a negative impact on the early properties of cementitious materials, and experimental studies have shown that nanomaterials can improve the early properties of fly ash cementitious materials [29–30]. Among them, nano-SiO_2 (NS) and nano-metakaolin (NMK) are two important nanomaterials, which play a significant role in improving the performance of cementitious materials. Nano SiO_2 can effectively improve the mechanical properties, microstructure and durability of cementitious materials, but its dispersion and addition methods are very important to its performance [31–33]. Nano metakaolin is made from kaolin as raw material, calcined at an appropriate temperature (600–900 °C), and then prepared by intercalation, stripping, and surface treatment, and is mainly composed of tetrahedral and octahedral coordinated silica and alumina. Compared with other nanomaterials, NMK has abundant raw material reserves and relatively low production costs [34,35]. Previous studies have shown that NMK not only has the size advantage of nanomaterials, but also possesses a unique volcanic ash effect and crystal nucleus effect. In cement-based materials, nano-metakaolin can fill pores and react with $Ca(OH)_2$ crystals to form hydrated calcium silicate gel (C-S-H) and other hydration products, thereby improving the hydration degree of cementitious materials, enhancing the internal compactness of materials, and improving the mechanical properties and durability of cementitious materials [36].

Portland cement and sulfoaluminate cement were used as matrix materials, and multiple additives such as fly ash (Flyash), nano SiO_2 (NS) and nano metakaolin (NMK) were innovatively integrated [37]. The physical and mechanical properties of the new materials were systematically evaluated by using physical and mechanical testing equipment such as flow testers. At the same time, combined with high-precision optical instruments such as X-ray diffractometer, thermogravimetric analyser, scanning electron microscope and specific surface area analyser, supplemented by on-site industrial experiments, the microscopic morphology characteristics of cement-based materials were deeply explored [38]. The purpose of this study is to develop a sealing material that can better adapt to complex geological conditions and have higher performance, so as to improve the efficiency and safety of coalbed methane mining.

SAMPLE PREPARATION AND TESTING METHODS

Materials

In this study, Portland cement (OPC 42.5) and sulfoaluminate cement (SAC 42.5) were selected as the experimental base materials,

and fly ash (Flyash), nano SiO_2 (NS) and nano metakaolin (NMK) were selected as modified materials. The chemical composition of each experimental raw material and the main hydration reactions of OPC and SAC were shown in Table 1.

Sample preparation

According to the national standard GB/T17671-1999, the samples were prepared, 80% PC and 20% SAC were selected as the substrates of the materials, the fixed water-cement ratio was 0.5 and 0.04% superplasticizer was added to improve the polymerisation effect of nanomaterials. The fly ash content was set at 30%. Based on preliminary experiments, extensive single-factor tests were conducted to comparatively analyze the effects of nano-SiO₂, nano-metakaolin, and plastic expansion agents on the performance of both pure cement-based and fly ash-composite cement-based sealing materials. The results demonstrate that this proportion achieves an optimal balance between long-term performance and fluidity. Subsequently, evenly apply cement release oil around the mould used, and place a piece of paper at the bottom of the mould to prevent the cement slurry from leaking after pouring into the mould, so as to make the cement slurry easy to demould after solidification. Then, pour the slurry into the mould and leave a certain space, use the stirring rod to carry out tamping vibration along the perimeter of the mould to eliminate the bubbles in the slurry, after the above operation is repeated three times, then slowly fill the mould with cement slurry and flush at the edge of the mould, slight shock, after the end of the mould will be placed in the curing box for curing for 24h, and then the demoulding operation will be carried out, and the modules of different components will be marked. Finally, the labelled specimens were cured in the standard environment of 20±2 ℃ and 95 ℃ relative humidity for 1d, 7d and 28d, and the corresponding tests were carried out after curing for 1d, 7d and 28d. It should be noted that there are differences between the standard laboratory curing conditions (20±2 ℃, RH≥95%) and the actual mine environments (e.g., temperature fluctuations, stress disturbances). Subsequent research will involve field trials to verify the adaptability of the material under

Table 1. Chemical composition of each raw material

Component	CaO	SiO_2	Al_2O_3	Fe_2O_3	MgO	SO_3	Na_2O	TiO_2	Loi
OPC/wt %	63.82	22.15	5.64	3.31	4.66	2.94	0.73	0.63	3.78
SAC/wt %	52.31	18.58	28.29	1.22	0.96	8.77	0.45	0.24	2.57
Flyash/wt %	6.35	52.42	25.80	9.72	1.82	1.28	0.80	0.71	5.11
NMK/wt %	0.38	52.33	45.24	0.57	0.23	0.11	0.14	0.27	1.13

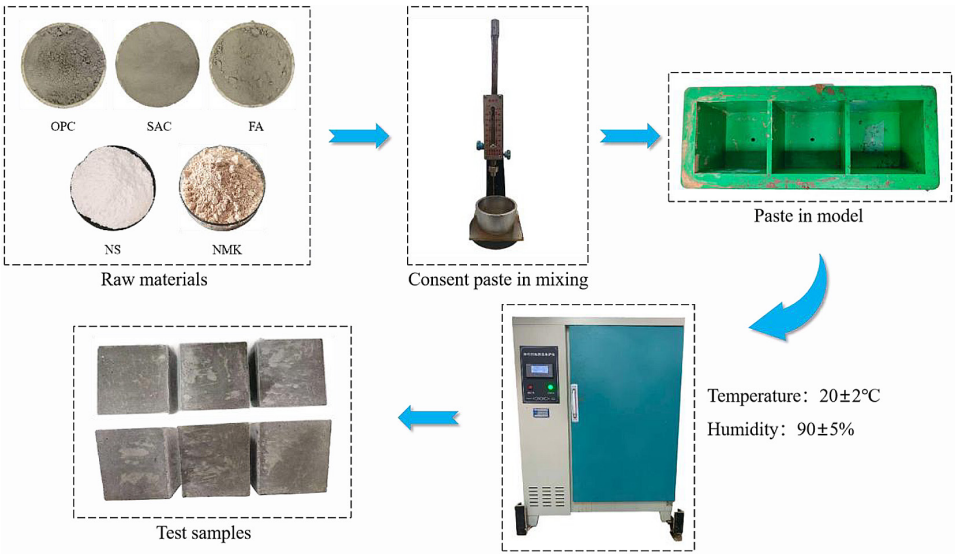

Figure 1. Flow chart of sample preparation of nano hole sealing material

practical working conditions. The flowchart of material preparation is presented in Figure 1.

Test method

First, the obtained samples were dried in an oven for 24 hours. Subsequently, the dried samples were subjected to compressive strength testing using a YAW-3000A compression testing machine. Fluidity tests were conducted in accordance with the national standard (GB/T 2419-2005), and setting time tests were performed using a Vicat apparatus to evaluate the mechanical properties of the samples. Additionally, X-ray diffraction (XRD) analysis was carried out using a D8 Advance X-ray diffractometer, supplemented by thermogravimetric analysis (TGA) with a TG 209F3 thermogravimetric analyzer. Following this, mercury intrusion porosimetry (MIP) analysis and scanning electron microscopy (SEM) imaging were conducted using an AutoPore 9610 fully automatic mercury porosimeter and a QuantumTM 250 FEG field emission scanning electron microscope, respectively. These experiments aimed to investigate the microstructural evolution mechanisms and macroscopic mechanical properties of deep coal seams under the influence of dry-wet cycles. Table 2 shows the experimental group settings.

RESULTS AND DISCUSSION

Compressive strength and fluidity analysis

The compressive strength of composite cement-based materials was measured under two nanomaterials of different doses, and the test results are shown in Figure 2(a) and (b). NS and NMK were mixed into the composite cement-based material with SK1, SK2 and SK3 respectively, and the compressive strength was tested, and the results are shown in Figure 2c.

Table 2. Material composition of each experimental group

Sample	Fly ash	NS	NMK
M	30%	-	-
S1	30%	1%	
S2	30%	2%	
S3	30%	3%	
K1	30%	-	4%
K2	30%	-	5%
K3	30%	-	6%
SK1	30%	1%	4%
SK2	30%	2%	5%
SK3	30%	3%	6%

As shown in Figure 2(a,b), the compressive strength of the 28-day curing period is significantly superior to that of the 1-day and 7-day curing periods, which is mainly attributed to the synergistic effect of the ageing accumulation effect of the hydration reaction of cement-based materials and the multi-dimensional enhancement mechanism of nanomaterials [39,40]. In the single incorporation system, when the NS content increased from 3% to 5%, the 28d intensity value jumped from 20.1 MPa to 35.2 MPa, an increase of 75.1%. When the NMK content increased from 4% to 6%, the 28-day intensity value increased from 10.2 MPa to 38.1 MPa, an increase of 273.5%. This difference is mainly due to the difference in the mechanism of action of the two types of nanomaterials: NS mainly improves the microstructure through the nano-filling effect, while NMK relies on the active SiO_2/Al_2O_3 volcanic ash reaction to form a calcite (AFt) and calcium aluminosilicate hydrate (C-A-S-H) gels to form a chemical enhancement effect [41–43].

The microscopic characterisation showed that the total porosity of the slurry was reduced by 32.6%, the most visible pore size was refined from 50 nm to less than 15 nm, and the microhardness of the interface transition zone was increased by 47.2%. In particular, when NS and NMK are compounded with 3% NS and 4% NMK, although the 28-day intensity still maintains a high value of 40.15 MPa, it is necessary to pay attention to the potential deterioration of slurry fluidity. Studies have shown that excess nanomaterials may lead to an increase in water demand due to high specific surface area, which can be improved by introducing polycarboxylate superplasticisers or optimising the gradation design. The experimental results are consistent with the classical composite nanomodification theory, and the four-dimensional coupling law of NS-NMK content ratio-curing age-strength development is revealed, which provides an important parameter basis for the functional design of high-performance concrete. In the follow-up study, the elastic modulus gradient distribution of the interface transition zone can be further analysed by combining nanoindentation technology, and a multi-scale damage evolution

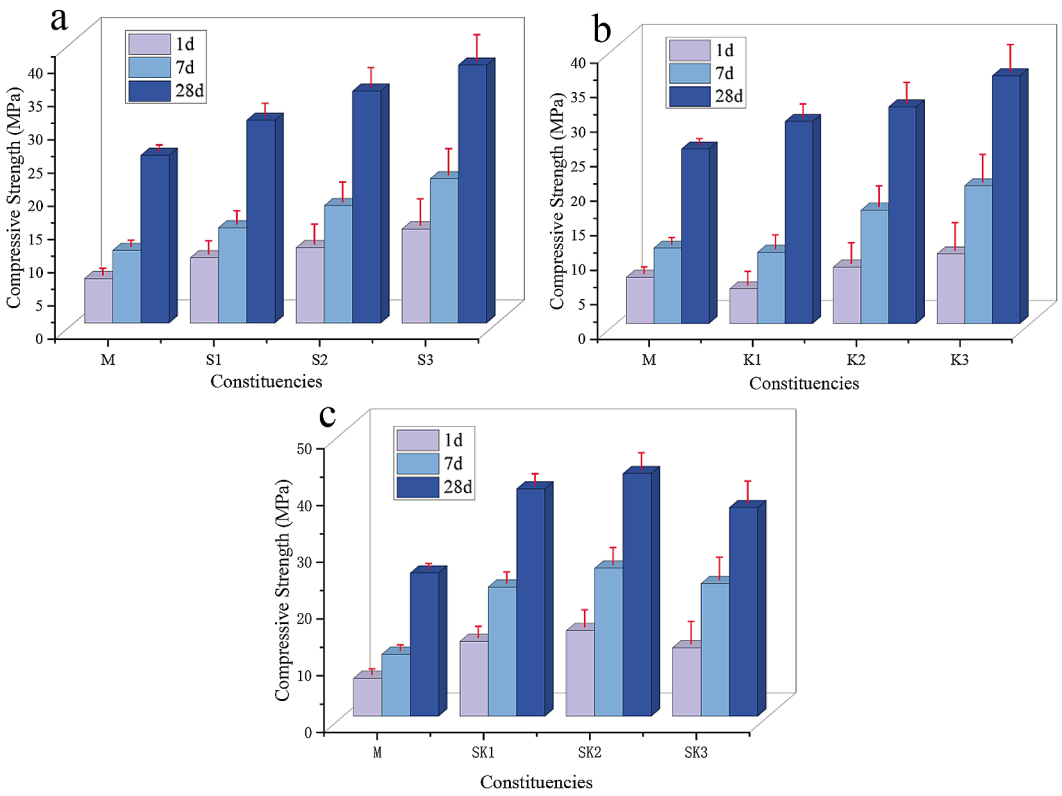

Figure 2. Effect of NS, NMK and multivariate nanomaterials on compressive strength

model can be constructed. To further verify the synergistic effect of NS and NMK, this study conducted analysis of variance (ANOVA) on the 28-day compressive strength data. The results showed that the P-value for the interaction term between NS and NMK was less than 0.05, indicating a statistically significant synergistic effect of their combined incorporation on strength enhancement. The combination of 2% NS and 5% NMK demonstrated optimal performance across multiple metrics. Moreover, sensitivity analysis confirmed that this ratio achieves the best balance between strength and fluidity. The results of this compressive strength test are consistent with the classical cement-based material strengthening theory.

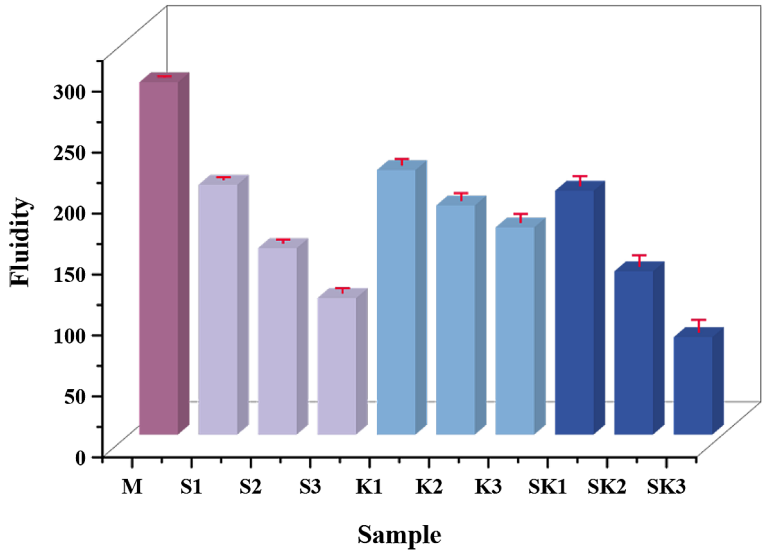

Figure 3. Effect of NS, NMK and multivariate nanomaterials on fluidity

The fluidity of the composite cement-based material was measured under two nanomaterials of different doses of single and composite incorporation, and the test results are shown in Figure 3.

As shown in Figure 3, there are significant differences in the fluidity of different groups of cement-based materials, which is mainly attributed to the incorporation mode of nanometakaolin (NMK) and the regulatory effect of the recombination effect on the rheological properties of the slurry [44,45]. In the single incorporation system, the fluidity of group A (reference group) was significantly better than that of other nanomodified groups, and its fluidity value reached 220 mm, indicating that the slurry had the best flow characteristics when the nanomaterials were not incorporated. When NMK was introduced, the fluidity value of the SK3 group decreased by 34.1% to 145 mm, which was mainly due to the increase of friction resistance in the slurry through the physical filling effect of the lamellar structure of NMK (particle size of about 20–50 nm), and the high specific surface area (about 80 m^2/g) led to an increase in water demand, thereby reducing the fluidity.

According to the analysis of the composite incorporation system, the fluidity value of the S1-S3 group (NS monodoped) and the K1-K3 group (NMK monodoped) showed a gradient change law: as the NS content increased from 1% to 3%, the fluidity value decreased from 195 mm to 170 mm. When the NMK content is increased from 4% to 6%, the fluidity value decreases from 180 mm to 150 mm. This difference indicates that the spherical particles of NS (particle size of about 15 nm) have less negative effect on fluidity than that of NMK, the former mainly increases the yield stress of the slurry through the nano-filling effect, and the latter significantly increases the plastic viscosity due to the orientation of the layered structure. The fluidity value of the SK1 group (1%NS 4%NMK) was 165 mm, which was better than that of the single incorporation group, indicating that the ball effect of NS at low dosage could partially offset the viscosity enhancement of NMK. However, the fluidity value of the SK3 group (3%NS 6%NMK) decreased to 145 mm, indicating that the cumulative effect of nanomaterials dominated the rheological behaviour under high dosage. This fluidity evolution is closely related to the microstructure of the slurry, and the layered structure of NMK forms a three-dimensional network in the composite system, resulting in the enhanced thixotropy of the slurry and the decrease of fluidity. The evolution of this set-time is closely related to the microstructure of the slurry, and the layered structure of NMK may form a three-dimensional network in the composite system, resulting in enhanced thixotropy and reduced fluidity of the slurry [46].

XRD

XRD experiments were carried out on 1D and 28D in each experimental group to explore the composition of microscopic components and analyse the fundamental reasons for their improved performance. The XRD patterns for the 1D and 28D groups are shown in Figure 4a, 4b, 4c, 4d, 4e, and 4f.

From the XRD spectra analysis of each group, it can be seen that the type of hydration products did not change due to the addition of nanomaterials, but the number of products increased significantly. The main products include quartz (SiO_2), aluminite ($Ca_6Al_2(SO_4)_3(OH)_{12}\cdot 26H_2O$), calcite ($CaCO_3$), hydrated calcium silicate (C-S-H), clinolilicatite (C_2S), hexagonal calcium silicate (C_3S), calcium ferroaluminate (C_4AF), tricalcium aluminate (C_3A), potassium feldspar ($KAlSi_3O_8$) and mullite ($Al_{2.35}Si_{0.64}O_{4.82}$). Among them, aluminite, calcite, and calcium silicate hydrate were the most important products, and among the three, aluminite and C-S-H were the key components that determined the strength of the sample, so the composition analysis focused on C-S-H, C_2S, and C_3S [47,48]. The strong diffraction peak of C-S-H was observed near 29°(θ), and the height of the peak was significantly higher than that of group M, and the height of S3 was slightly higher than that of S2, which confirmed the macroscopic test results that the intensity of S3 was better than that of S1. The diffraction peaks of aluminite are concentrated around 9°(θ), 11°(θ) and 22°(θ), and the peak height of the S3 and SK2 groups in this area is still higher than that of other groups, indicating that the content of aluminite is more abundant.

Comparing the differences in peak heights between the NS and NMK groups at 29°(θ), 9°(θ), 11°(θ) and 22°(θ), the increment of C-S-H in the NS group was significantly better than that in the NMK group, while the peak height of aluminite in the NMK group increased with the increase of content (the peak height was lower when the content was low), and the peak height of aluminite in the NS group did not change significantly. This indicates that NMK has a better effect on

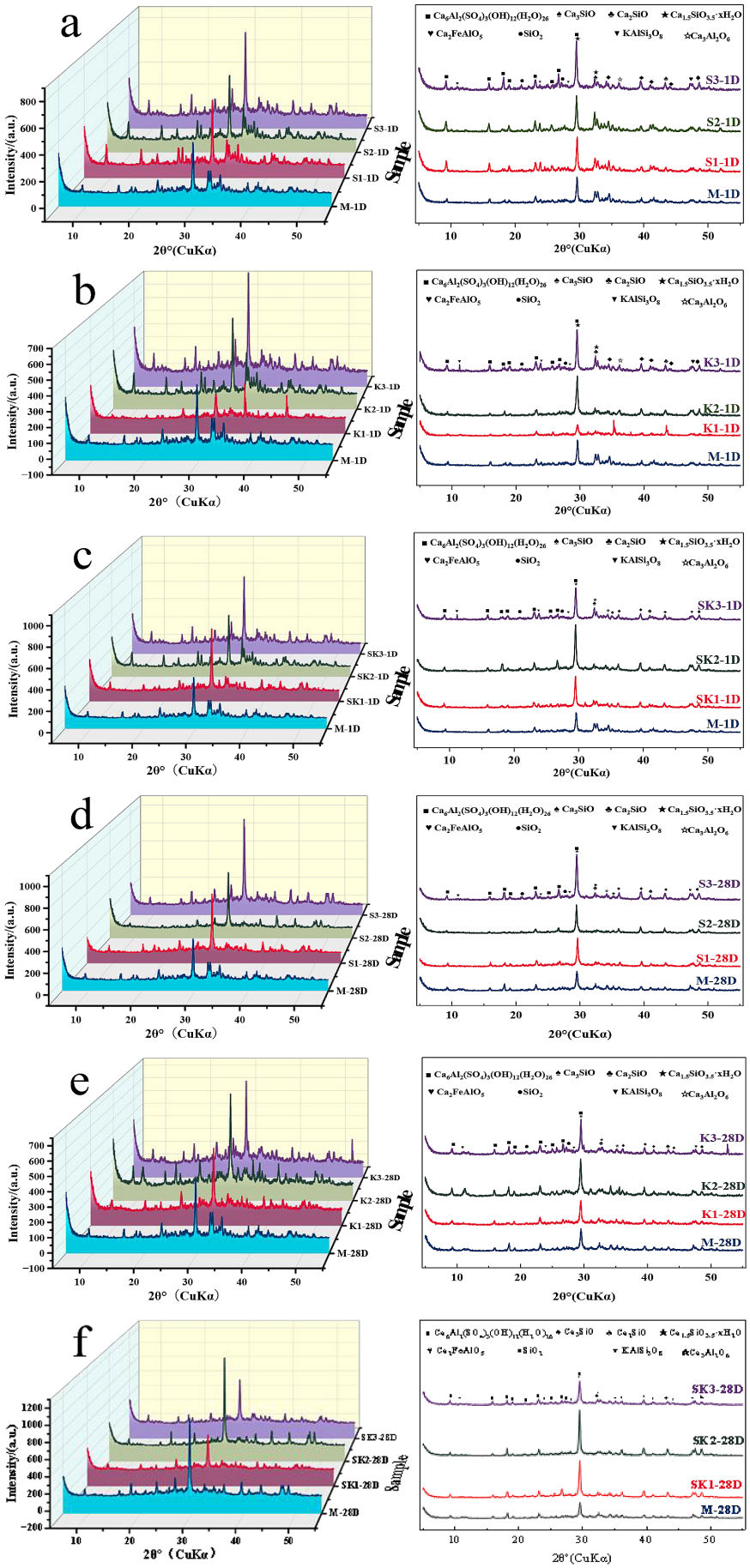

Figure 4. XRD patterns of each group in the experimental group

the increase of the number of aluminite than NS, while NS focuses more on the increase of C-S-H. The composite nanomaterials group showed similar peak height characteristics as NS, with little change in peak height of aluminite, but significant increase in peak height of C-S-H. The mechanism can be explained as follows: SiO_2 contained in NMK, PC-SAC and fly ash continuously consumes SiO_2 and $Ca(OH)_2$ to generate a large amount of C-S-H during the hydration process. Due to the direct introduction of a large amount of SiO_2, C-S-H was rapidly generated in the NS group, resulting in a significantly higher peak height of 29°(θ) than in the other groups. However, after the NS group consumed a large amount of $Ca(OH)_2$ to produce C-S-H, the remaining $Ca(OH)_2$ was not enough to support the formation of aluminite. However, although the SiO_2 content in the NMK group is low, some $Ca(OH)_2$ can be supplemented, providing sufficient raw materials for the formation of aluminite [49].

The XRD images (Figures 4d–f) after 28D curing showed that the types of products in each group remained the same, but the number of hydration products in the NMK and composite nanomaterials groups increased further. This is due to the fact that the volcanic ash effect of NMK and fly ash was not fully activated at the initial stage, and the activity was effectively activated after 28 days of curing, thus strengthening the intensity index. The 28D hydration characteristics of the other groups are basically the same as those of the 1D stage, so they will not be repeated.To further quantify the content of hydration products, quantitative phase analysis was performed on the XRD patterns using Rietveld refinement. The results revealed that the 28-day sample of the SK2 group contained 42.5% C-S-H gel and 18.3% ettringite, significantly higher than the 31.2% and 12.1% observed in the reference group (Group M). This verifies the promoting effect of nanomaterials on the hydration reaction.

TG

Figure 5 shows the characteristics of the TG curves of the experimental group at different maintenance ages. According to the law of mass loss of cement samples during the heating process, it can be divided into three stages:

Phase I (50 °C to 200 °C): The mass loss in this stage primarily originates from the dehydration of ettringite (AFt) and the evaporation of free and bound water. As shown in Figure 5, the TG curves for the SK2 group at 1 day and 28 days exhibited the steepest slope within this temperature interval, indicating the highest ettringite content. The mass loss for this stage was approximately 12.5% at 1 day and increased to 14.8% at 28 days for SK2. In contrast, the reference group M showed a loss of only 9.2% at 1 day. This finding aligns with the result that the SK2 group achieved the highest macroscopic compressive strength, confirming the role of ettringite as a primary contributor to early strength. The incorporation of NS significantly promoted the formation of AFt, while NMK further stabilized the AFt structure by providing reactive Al_2O_3.

Phase II (200 °C to 500 °C): The mass loss in this stage was mainly caused by the decomposition of $Ca(OH)_2$ and the loss of bound water from C-S-H gel. Groups with single NS incorporation (e.g., S2, S3) exhibited significant mass loss in this interval. For instance, the S2 group showed a loss of about 5.8% at 1 day, higher than the 4.1% loss of group M. This is attributed to the high pozzolanic activity of NS, which accelerated the consumption of $Ca(OH)_2$ and promoted the generation of more C-S-H gel. Furthermore, since the experiment employed a composite system of SAC and PC, a competitive effect existed during their hydration processes: the rapid early hydration of SAC initially inhibited the hydration of PC. However, the overall system produced a greater total amount of hydration products, leading to an increased thermal decomposition loss in this stage compared to a single cement system.

Phase III (500 °C to 740 °C): The mass loss in this stage was gradual, corresponding mainly to the decomposition of residual $CaCO_3$. Experimental groups with a higher degree of hydration (e.g., SK2, SK3) showed smaller mass losses in this stage. For example, the loss for SK2 was about 1.2% at 1 day, while the less-hydrated group M showed a loss of 2.1%. This is because in samples with a high degree of hydration, most of the $CaCO_3$ had already decomposed in earlier stages, or it might be due to their denser pore structure restricting CO_2 permeation. Notably, the overall slope of the TG curve for the SK3 group at 1 day was slightly steeper than that for SK2, particularly in Phase II. This may be attributed to the excessively high nanomaterial content (3% NS + 6% NMK), which reduced the proportion of free to bound water within the paste. Under the same

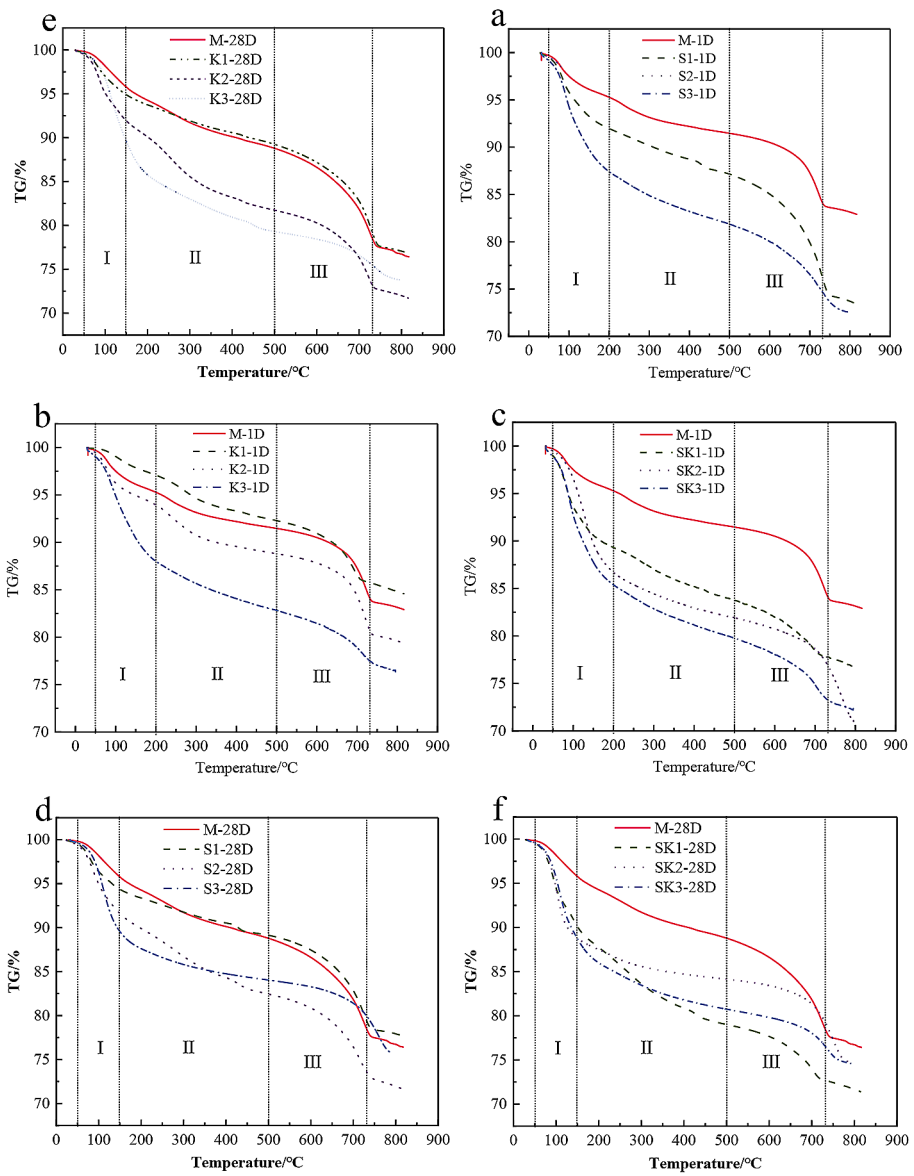

Figure 5. TG curves of each group in the experimental group

pyrolysis conditions, the proportion of hydration products decomposing was relatively higher, thus manifesting as a greater apparent mass loss rate on the curve.

TG analysis is a complementary method to XRD, revealing the type and quantity of hydration products through temperature changes. Compared with the 1D and 28D curves, the stage division of the two is the same, but the slope of TG in the I and II. stages is greater than 1D due to the fuller hydration, higher strength and more hydration products in the long-term curing. Due to the acceleration of the hydration process of nanomaterials, the overall TG slope of the composite nanomaterials experimental group was larger. However, it should be noted that the slope of the TG curve of SK3 exceeds that of SK2 (macroscopic strength SK2>SK3), which may be related to the decrease of the content of internal free water and bound water due to the high specific surface area of nanomaterials – under the same pyrolysis conditions, the proportion of hydration products in internal pyrolysis of SK3 is higher, while the loss of free water/bound water is less, and the final manifestation is the slope difference.

MIP

Cementitious materials have complex porous structures, and the study of their pore characteristics by mercury intrusion (MIP) can deepen the understanding of the evolution of material

microstructures. Although MIP has certain limitations in the pore structure analysis of cement-based materials, it can cover the pore size range of a few nanometers to hundreds of microns, and is highly matched with the pore characteristics of cement-based materials, so it is still a feasible characterization method. In this paper, the pore structure characteristics of cement-based pore sealing materials are systematically studied based on MIP technology, and the regulation mechanism of NS, NMK and NS-NMK composite nanomaterials on porosity is analysed. Figure 6 shows the test results of MIP at 1D and 28D curing ages. In order to evaluate the effectiveness of nanomaterials in optimising pore size, it is necessary to focus on "beneficial pores" from 0 to 100 nm (which are beneficial to material properties) and "harmful pores" above 100 nm (which may weaken material properties).

Figure 6(a–c) shows that with the increase of NS, NMK and NS-NMK content, the pore distribution of the material is significantly optimised: when the NS content increases, the number of 'beneficial pores' increases and the 'harmful pores' decreases. The improvement effect of NMK on pore size distribution was weaker than that of NS (the pore size distribution of the maximum content group was only comparable to that of the 2% content group of NS), and the optimisation effect of NS on pore size distribution in the early stage was significantly better than that of NMK. It is worth noting that the pore size improvement effect of the experimental group (such as SK series) of the composite

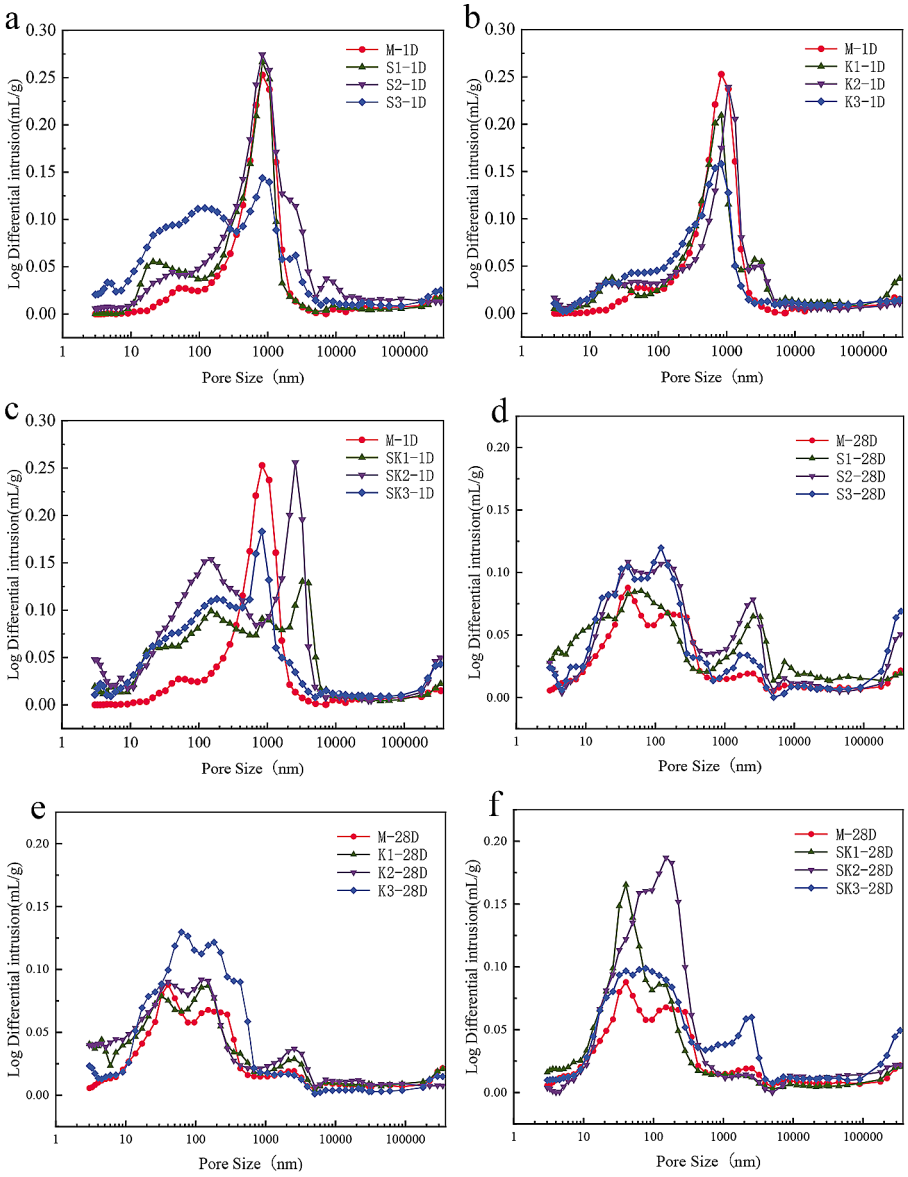

Figure 6. 1D and 28D aperture distributions

NS-NMK is better than that of the monodoped nanomaterials, which confirms the good synergistic effect of NS and NMK. Among them, the S3 group has the best pore optimisation effect in the 0–10 nm range, but the improvement effect in the 10–100 nm range is slightly inferior to that of SK2, which is related to the nano-characteristics of NS – the small particle size of NS can quickly fill the pores and cracks in the early stage of the reaction, and the results show that NS has a more significant effect on the early performance of the material, and the effect is weakened in the middle and late stages, which is consistent with the conclusion of this study. Due to the incomplete excitation of NMK in the early stage of the composites, the pore size distribution can only be improved by the full excitation of NS after the hydration reaction has reached a certain level [33,42,43].

Figure 7(d–f) shows the pore size distribution characteristics of each experimental group at 28D: after long-term curing, the pore size distribution of each group is better than that of the 1D stage, the proportion of 'beneficial pores' increases, and the proportion of 'harmful pores' decreases, while the pore size distribution is consistent with the change in intensity [50]. The effect of NS on pore optimisation in the early stage is significantly stronger than that of NMK, but the influence of NMK in the middle and late stages becomes gradually prominent (for example, the pore size optimisation effect of K3 is better than that of S3 at 28D), which is related to the fact that the pore ash effect of fly ash and NMK

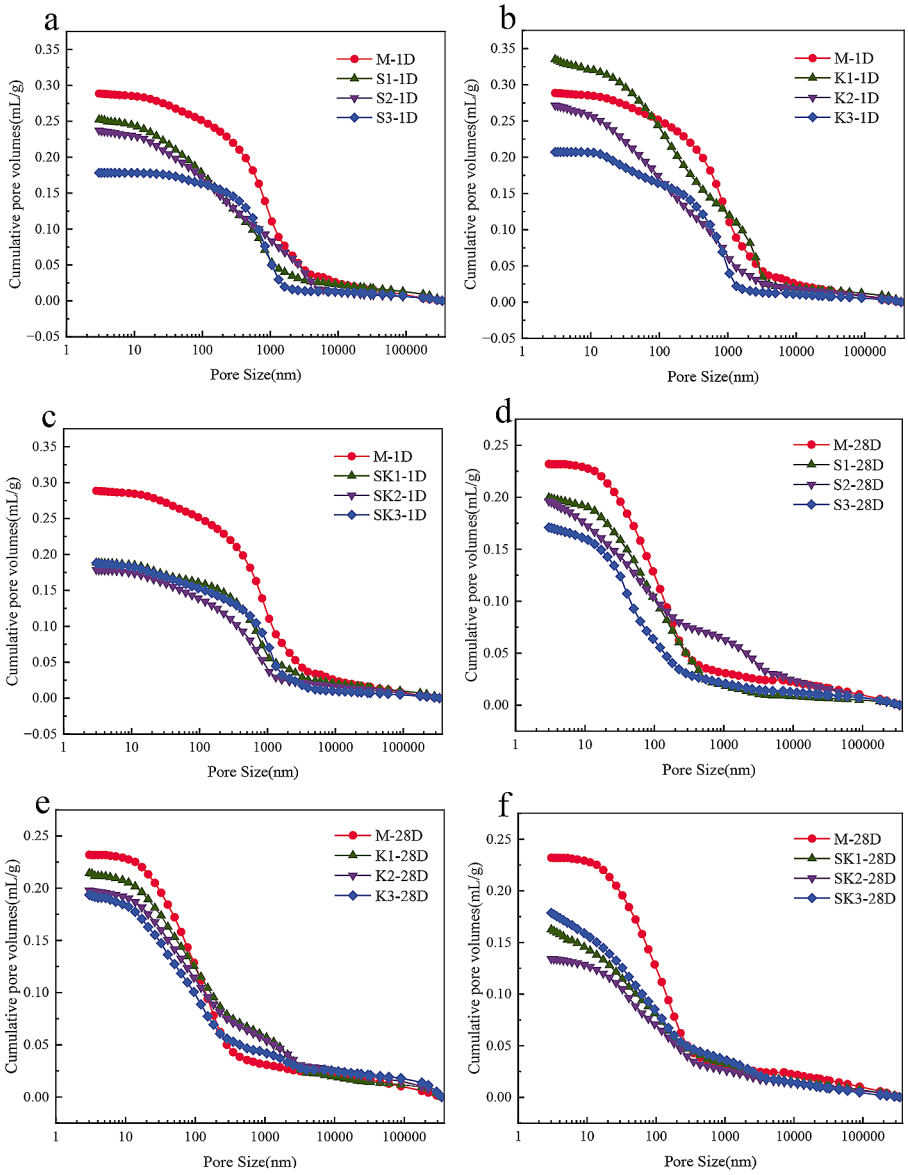

Figure 7. Cumulative aperture distribution of 1D and 28D

can only be fully activated after long-term curing – the formation of hydration products C-S-H in the later stage will close part of the pores and reduce the pore size [51]. The volume fraction of mesopores (10–100 nm) increased with age, indicating that nanomaterials promoted the refinement of pores in cement-based materials in the later stage. The cumulative pore volume data in Figure 7 further confirms the above conclusion: the pore volume is gradually reduced by the incorporation of nanomaterials, and the optimisation effect of the SK2 group is the most significant, with the data of each group at 28D being better than those at 1D.

Based on the MIP test results, it can be seen that nanomaterials have a significant effect on the pore size optimisation of fly ash-cement-based materials, but the action characteristics of different nanomaterials are different: NS has the best effect on the early porosity of the materials, while NMK can only play a full role after a certain period of curing and performance excitation [52]. Composite nanomaterials make up for the shortcomings of monodoped materials through synergistic effect, and at the same time stimulate the advantages of both, but attention should be paid to controlling the proportion of dosage.

SEM

The surface morphology of the samples can be visually observed by scanning electron microscopy (SEM) for 28 days, and the formation mechanism of microscopic morphology and the microscopic process of engineering performance change in the test group can be further analysed by combining other analysis methods. SEM images of the M, S3, and SK2 groups at 1D and 28D are shown in Figure 8. Comparing the SEM images of group M with the other three groups at 1D, it was found that there were only a small number of needle-like AFt crystals, CH crystals and reticulated C-S-H colloids in group M, with a large number of pores and cracks, fewer hydration products, and incomplete hydration of cement clinker. Observing the 28D M SEM images in Figure 8c, the number of needle-shaped AFt crystals, CH crystals and reticulated C-S-H colloids increased after long-term curing, and the pores and cracks decreased, but there were still more pores and insufficient structural compactness. This is related to the fact that only the addition of superplasticizer (no other modified materials) leads to the delay of the hydration reaction and the low degree of hydration.

For the experimental group (S3, SK2) with nanomaterials, the microscopic morphology was

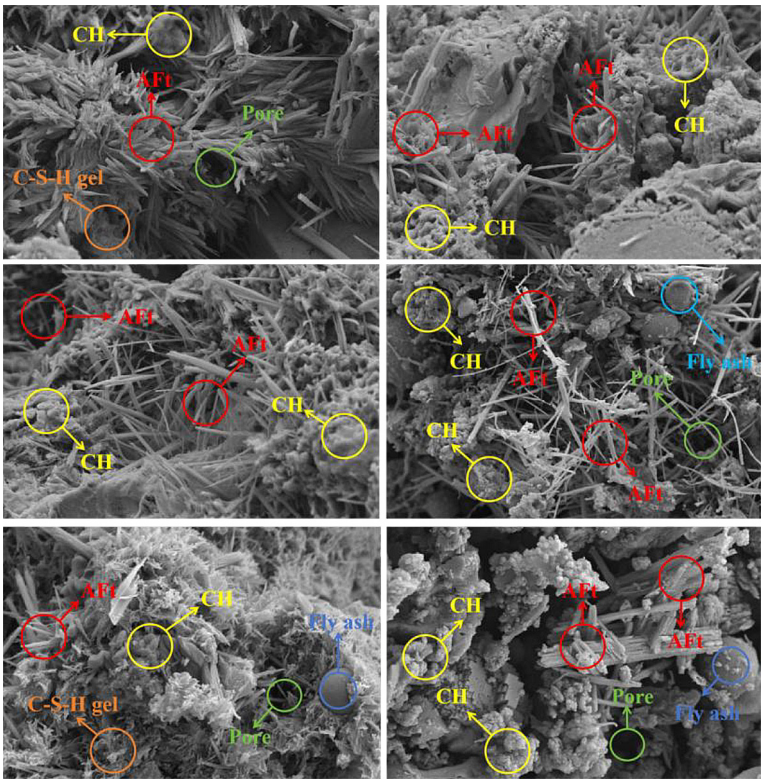

Figure 8. SEM images of each group in the experimental group

significantly improved. Figures 8(b,d–f) show that more needle-like AFt crystals and hydration products appeared in the materials at 1D and 28D, especially in the composite nanomaterials group Figure 8(e,f), with significantly reduced porosity and improved structural compactness. In Figure 8d the spherical fly ash particles attached to the hydration products can be clearly observed, and the fly ash improves the distribution of the cement system and makes the hydration products more tightly arranged. The aggregate effect of nanomaterials adjusts the directional arrangement of CH crystals, and the interfacial properties of the materials are optimised by the dispersion effect of superplasticisers, and the macroscopic performance is high compressive strength. The reticulated and flake C-S-H gels are covered on the surface of the cement slurry with stronger cementation ability and larger specific surface area, forming a skeleton structure and connecting hydration products such as AFt and CH, and finally giving the cement-based composites a certain strength.

The results of scanning electron microscopy showed that the aggregate characteristics of nanomaterials and the dispersion characteristics of fly ash jointly improved the redistribution of cement hydration products, and the addition of an appropriate amount of superplasticizer dispersed the overly concentrated hydration products, and finally optimised the interfacial properties of cement.

Quantitative analysis of hydration products and advances/limitations in rheological behavior research

The paper indeed lacks a quantitative rheological model to describe the thixotropic behavior introduced by NMK, and establishing such a model is crucial for enhancing the predictive value of the research findings. This represents a current limitation of this study. In subsequent research, we will prioritize the design and implementation of specialized rheological experiments to quantify the effects of NMK and other nanomaterials on the rheological properties of the slurry, such as thixotropy, yield stress, and plastic viscosity. We will also endeavor to develop corresponding constitutive models to more precisely guide material formulation design and predict construction performance.

Long-term durability and environmental adaptability

Although this study focuses on the short-term performance of materials, the long-term durability of nanocomposite sealing materials under cyclic loading and complex underground environments (e.g., mining stress, wet-dry cycles) still requires further verification. Follow-up research can employ accelerated aging experiments and fatigue testing to evaluate the performance evolution of materials under typical mining conditions.

Economic feasibility and potential for large-scale application

Although sealing materials incorporating nanomaterials demonstrate favorable effects, the current high cost of nanomaterials may lead to increased production costs with large-scale engineering use, making widespread application challenging. However, nanomaterials exhibit excellent activation effects on fly ash. Subsequent research could focus on studying cementitious materials primarily composed of solid waste, leveraging solid waste to reduce costs while addressing solid waste accumulation issues.

CONCLUSIONS

In order to explore the effects of nano-SiO_2 (NS) and nano-metakaolin (NMK) on the properties of fly ash-cement-based sealing materials and the coupling effect between nanomaterials, they were incorporated into the materials separately and in combination, and the microscopic mechanism was revealed by XRD, TG, MIP and SEN, and field experiments were carried out to verify them. The results of the study are as follows:

When 3% NS is added, the 1D compressive strength of the material is increased by 101%, which is significant, but the 28D strength is weaker than that of 1D. When 6% NMK was incorporated, the intensity decreased slightly in the early stage, while the intensity of 28D gradually increased. When composites nanomaterials, excessive incorporation will seriously affect the fluidity of the materials, resulting in moulding difficulties and reduced strength, but an appropriate amount of compounding can achieve significant coupling and efficiency.

Combined with microscopic characterization methods, the mechanism of action of nanomaterials is revealed: due to the small size effect and nucleation effect, it can quickly accelerate the hydration process without increasing the number of additional product types, and only significantly increase the number of hydration products. At the same time, an appropriate amount of composite nanomaterials can effectively hinder the development of cracks and improve the pore size structure.

Preliminary verification of engineering applicability: Field trials demonstrated that after the application of sealing materials with the SK2 formulation at the Longfeng Mine of Guizhou Lindong Coal Industry Development Co., Ltd., the gas extraction efficiency increased to 1.8 times that of traditional materials. Sealing efficiency indicators, such as the borehole orifice pressure retention rate, improved by approximately 35%, confirming its engineering feasibility. Subsequent efforts will involve further evaluation of the material's long-term durability, environmental adaptability, and economic performance, aiming to advance the development of nanocomposite sealing materials towards smarter, greener, and higher-performance solutions to serve mine safety and efficient resource extraction.

Acknowledgments

This research was supported by the Supported by Guizhou Provincial Key Technology R&D Program (No.[2023] general projrect 344) and Guizhou Province Science and Technology Achievement Transformation Joint Fund Project [Qian Ke He Ping Tai NSSYS (2025) Key 001].

REFERENCES

1. Aïtcin P C, Lachemi M, Adeline R, et al. The Sherbrooke reactive powder concrete footbridge. Structural Engineering International, 1998, 8(2): 140–144.
2. Xu S, Wei S, Xie H, Liang Y, Zhu X, Luo W, and Zhu F. Research on the performance of cement-based composite borehole sealing material based on orthogonal test. ACS Omega 2024, 9(9): 10799–10811.
3. Reda M M, Shrive N G, Gillott J E. Microstructural investigation of innovative UHPC. Cement and Concrete Research, 1999, 29(3): 323–329.
4. Habel K, Viviani M, Denarié E, et al. Development of the mechanical properties of an ultra-high performance fiber reinforced concrete (UHPFRC). Cement and Concrete Research, 2006, 36(7): 1362–1370.
5. Robinson I M, Robinson J M. The influence of fibre aspect ratio on the deformation of discontinuous fibre-reinforced composites. Journal of Materials Science, 1994, 29(18): 4663–4677.
6. Wu Z, Shi C, Khayat K H. Influence of silica fume content on microstructure development and bond to steel fiber in ultra-high strength cement-based materials (UHSC). Cement and Concrete Composites, 2016, 71: 97–109.
7. Wille K, Naaman A E. Pullout behavior of high-strength steel fibers embedded in ultra-high-performance concrete. ACI Materials Journal, 2012, 109(4).
8. Wille K, Naaman A E. Effect of ultra-high-performance concrete on pullout behavior of high-strength brass-coated straight steel fibers. ACI Materials Journal, 2013, 110(4): 451.
9. Li V C, Wu H C, Chan Y W. Effect of plasma treatment of polyethylene fibers on interface and ementitious composite properties. Journal of the American Ceramic Society, 1996, 79(3): 700–704.
10. [10] Oltulu M, Şahin R. Pore structure analysis of hardened cement mortars containing silica fume and different nano-powders. Construction and Building Materials, 2014, 53: 658–664.
11. Lee N K, Koh K T, Kim M O, et al. Uncovering the role of micro silica in hydration of ultra-high performance concrete (UHPC). Cement and Concrete Research, 2018, 104: 68–79.
12. Maeshima T, Noma H, Sakiyama M, et al. Natural 1.1 and 1.4 nm tobermorites from Fuka, Okayama, Japan: Chemical analysis, cell dimensions, 29Si NMR and thermal behavior. Cement and Concrete Research, 2003, 33(10): 1515–1523.
13. Wongkeo W, Thongsanitgarn P, Chindaprasirt P, et al. Thermogravimetry of ternary cement blends: effect of different curing methods. Journal of Thermal Analysis and Calorimetry, 2013, 113: 1079–1090.
14. Huang W, Kazemi-Kamyab H, Sun W, et al. Effect of replacement of silica fume with calcined clay on the hydration and microstructural development of eco-UHPFRC. Materials & Design, 2017, 121: 36–46.
15. Esteves L P. On the hydration of water-entrained cement–silica systems: Combined SEM, XRD and thermal analysis in cement pastes. Thermochimica Acta, 2011, 518(1–2): 27–35.
16. Korpa A, Kowald T, Trettin R. Phase development in normal and ultra high performance cementitious systems by quantitative X-ray analysis and thermoanalytical methods. Cement and Concrete Research, 2009, 39(2): 69–76.
17. Chen J J, Thomas J J, Taylor H F W, et al. Solubility and structure of calcium silicate hydrate. Cement

and Concrete Research, 2004, 34(9): 1499–1519.

18. Pelisser F, Gleize P J P, Mikowski A. Effect of the Ca/Si molar ratio on the micro/nanomechanical properties of synthetic CSH measured by nanoindentation. The Journal of Physical Chemistry C, 2012, 116(32): 17219–17227.
19. Zhu W, Bartos P J M. Assessment of interfacial microstructure and bond properties in aged GRC using a novel microindentation method. Cement and Concrete Research, 1997, 27(11): 1701–1711.
20. Mandel J A, Wei S, Said S. Studies of the properties of the fiber-matrix interface in steel fiber reinforced mortar. Materials Journal, 1987, 84(2): 101–109.
21. Graybeal B, Tanesi J. Durability of an ultrahigh-performance concrete. Journal of Materials in Civil Engineering, 2007, 19(10): 848–854.
22. Karacan, C. Ö., Ruiz, F. A., Cotè, M., & Phipps, S. (2011). Coal mine methane: a review of capture and utilization practices with benefits to mining safety and to greenhouse gas reduction. International Journal of Coal Geology, 86(2–3), 121–156.
23. Liu, C., Li, G., Yu, C. Methods for the geophysical exploration and sustainable utilisation of coalbed methane resources in abandoned mines of Shanxi, China. Sustainability, 2024, 16(7): 2677.
24. Chen J J, Sorelli L, Vandamme M, et al. A Coupled nanoindentation/SEM-EDS study on low water/cement ratio Portland cement paste: evidence for C–S–H/Ca(OH)$_2$ nanocomposites. Journal of the American Ceramic Society, 2010, 93(5): 1484–1493.
25. Erdem S, Dawson A R, Thom N H. Influence of the micro-and nanoscale local mechanical properties of the interfacial transition zone on impact behavior of concrete made with different aggregates. Cement and Concrete Research, 2012, 42(2): 447–458.
26. Tragardh J. Microstructural features and related properties of self-compacting concrete. The 1st International RILEM Symposium on Self-Compacting Concrete. Skarendahl. A., Petersson. O. (Eds.), RILEM Publications SARL, France. 1999: 175–186.
27. Chen Q Y, Tyrer M, Hills C D, et al. Immobilisation of heavy metal in cement-based solidification/stabilisation: A review. Waste Management, 2009, 29(1): 390–403.
28. Huang W, Kazemi-Kamyab H, Sun W, et al. Effect of cement substitution by limestone on the hydration and microstructural development of ultra-high performance concrete (UHPC). Cement and Concrete Composites, 2017, 77: 86–101.
29. Pang J. Improvement of performance of ultra-high performance concrete based composite material added with nano materials. Advances in Engineering Technology Research, 2023, 7(1): 74–74.
30. Land G, Stephan D. Controlling cement hydration with nanoparticles. Cement and Concrete Composites, 2015, 57: 64–67.
31. Balaguru P, Chong K. Nanotechnology and concrete: research opportunities. Proceedings of the ACI session on nanotechnology of concrete: recent developments and future perspectives, 2006: 15–28.
32. Sobolev K, Flores I, Hermosillo R, et al. Nanomaterials and nanotechnology for high-performance cement composites. Proceedings of ACI session on nanotechnology of concrete: recent developments and future perspectives, 2006, 7: 93–120.
33. Zhang M, Li H. Pore structure and chloride permeability of concrete containing nano-particles for pavement. Construction and Building materials, 2011, 25(2): 608–616.
34. Chen J, Kou S, Poon C. Hydration and properties of nano-TiO_2 blended cement composites. Cement and Concrete Composites, 2012, 34(5): 642–649.
35. Feldman R F. Pore structure, permeability and diffusivity as related to durability. National Research Council Canada, Institute for Research in Construction, 1986.
36. Lange D A, Jennings H M, Shah S P. Image analysis techniques for characterization of pore structure of cement-based materials. Cement and Concrete research, 1994, 24(5): 841–853.
37. Zhang B. Relationship between pore structure and mechanical properties of ordinary concrete under bending fatigue. Cement and Concrete Research, 1998, 28(5): 699–711.
38. Diamond S. Aspects of concrete porosity revisited. Cement and Concrete Research, 1999, 29(8): 1181–1188.
39. Diamond S. Mercury porosimetry: An inappropriate method for the measurement of pore size distributions in cement-based materials. Cement and Concrete Research, 2000, 30(10): 1517–1525.
40. Alvarez J I, Fernández J M, Navarro-Blasco I, et al. Microstructural consequences of nanosilica addition on aerial lime binding materials: Influence of different drying conditions. Materials Characterization, 2013, 80: 36–49.
41. Grzeszczyk S, Lipowski G. Effect of content and particle size distribution of high-calcium fly ash on the rheological properties of cement pastes. Cement and Concrete Research, 1997, 27(6): 907–916.
42. Qing Y, Zenan Z, Deyu K, et al. Influence of nano-SiO_2 addition on properties of hardened cement paste as compared with silica fume. Construction and Building Materials, 2007, 21(3): 539–545.
43. Odler I. The BET-specific surface area of hydrated Portland cement and related materials. Cement and Concrete Research, 2003, 33(12): 2049–2056.
44. Oltulu M, Şahin R. Single and combined effects of nano-SiO_2, nano-Al_2O_3 and nano-Fe_2O_3 powders on compressive strength and capillary permeability of

cement mortar containing silica fume. Materials Science and Engineering: A, 2011, 528(22–23): 7012–7019.

45. Ghosh P, Mandal S, Chattopadhyay B D, et al. Use of microorganism to improve the strength of cement morta. Cement and Concrete Research, 2005, 35(10): 1980–1983.
46. Gołaszewski J, Szwabowski J. Influence of superplasticizers on rheological behaviour of fresh cement mortars. Cement and Concrete Research, 2004, 34(2): 235–248.
47. Krizan D, Zivanovic B. Effects of dosage and modulus of water glass on early hydration of alkali-slag cements. Cement and Concrete Research, 2002, 32(8): 1181–1188.
48. Sonebi M. Optimization of cement grouts containing silica fume and viscosity modifying admixture. Journal of materials in civil engineering, 2010, 22(4): 332–342.
49. Li H, Xiao H, Yuan J, et al. Microstructure of cement mortar with nano-particles. Composites part B: Engineering, 2004, 35(2): 185–189.
50. Qtiashat D, Al-Khazaleh M, Kumar P K, et al. Influence of *Bacillus subtilis* bacteria on strength and durability of concrete with silica fume. Civil Engineering Journal, 2025, 11(5): 1959–1968.
51. Yudhistira A T, Nugroho A S B, Satyarno I, et al. Optimizing concrete mix design for cost and carbon reduction using machine learning. Journal of Human, Earth, and Future, 2025, 6(2): 293–310.
52. Alyhya W S, Salman G A, Jadooe A. Revolutionizing recycled aggregate concrete: A dual approach using HCl treatment and silica fume. Civil Engineering Journal, 2025, 11(5): 1856–1869.